Remote Sensing of Environment 147 (2014) 65–78

Contents lists available at ScienceDirect

Remote Sensing of Environment

journal homepage: www.elsevier.com/locate/rse

Evaluation of the Interactive Multisensor Snow and Ice Mapping System (IMS) for monitoring sea ice phenology

Laura C. Brown [a,*], Stephen E.L. Howell [a], Jonas Mortin [b], Chris Derksen [a]

[a] Climate Processes Section, Climate Research Division, Environment Canada, 4905 Dufferin Street, Toronto, ON M3H 5T4, Canada
[b] Department of Meteorology and Bolin Centre for Climate Research, Stockholm University, SE-106 91 Stockholm, Sweden

ARTICLE INFO

Article history:
Received 23 September 2013
Received in revised form 18 February 2014
Accepted 20 February 2014
Available online 22 March 2014

Keywords:
Sea ice
IMS
QuikSCAT
AMSR-E
SSM/I
Ice cover duration
Melt duration

ABSTRACT

We present an evaluation of the Interactive Multisensor Snow and Ice Mapping System (IMS) for monitoring northern hemisphere sea ice phenology. Analysts utilize a variety of datasets to manually derive the daily extent of snow, ice, water and land, available at both 24 and 4 km. The 4 km IMS product was assessed for 2004–2008 against several previously established melt/freeze algorithms using Scatterometer Image Reconstruction (SIR) SeaWinds/QuikSCAT (QuikSCAT) backscatter (σ°), Advanced Microwave Scanning Radiometer for the Earth Observing System (AMSR-E) brightness temperature (T_B) measurements, data from the Special Sensor Microwave/Image data (SSM/I) and sea ice concentrations derived from DMSP Special Sensor Microwave/Imager–Special Sensor Microwave Imager Sounder (SSMI–SSMIS) data (NASATeam dataset). The resolution possible with the 4 km IMS product allows for better spatial representation of sea ice along the coastlines, the ice edges and in the narrow channels of the Canadian Arctic Archipelago as compared to the microwave products. IMS detects open water earlier and freeze onset later than the automated microwave products, and also allows for the detection of opening, and the subsequent closing, of leads that the other datasets are unable to detect. Using RADARSAT-1 imagery for evaluation, IMS is shown to outperform the other datasets for the timing and extent of the first open water detection. IMS identified between 17 and 53% greater open water coverage than the other datasets in the narrow channels of the Northwest Passage (Barrow Strait). In order to further the use of IMS for sea ice applications, we derived two new spatial datasets using the full record of IMS data (4 km: 2004–present, 24 km: 1997–present): melt duration to open water (duration from melt onset detected with SSM/I passive microwave until open water detected by IMS) and first year ice cover duration (duration from freeze onset until open water, both detected by IMS).

1. Introduction

Sea ice plays a critical role in the surface energy budget because of its strong contrast in albedo compared to open water, which in turn modulates atmosphere–sea ice–ocean energy exchange, primarily through the ice–albedo feedback (e.g. Perovich, Light, et al., 2007; Perovich, Nghiem, Markus, & Schweiger, 2007). The sea ice–albedo feedback occurs when surface air temperatures increase over sea ice, driving a decrease in surface albedo, leading to an increased absorption of shortwave radiation that in turn further increases surface temperatures and accelerates the ice melt process (Curry, Schramn, & Ebert, 1995). The recent shift in the Arctic's sea ice cover from thick multi-year ice (MYI) to thinner seasonal first-year ice (FYI) (Maslanik, Stroeve, Fowler, & Emery, 2011), which requires less energy to melt, has increased the importance of the sea ice–albedo feedback (Hudson et al., 2013; Perovich, Light, et al., 2007). Additionally, the date of melt onset over the Arctic sea ice is occurring earlier (e.g. Markus, Stroeve, & Miller, 2009), which enhances the sea ice–albedo feedback as an early melt onset increases the amount of cumulative solar energy absorbed by approximately 8.7 MJ m^{-2} day^{-1} throughout the melt season (Perovich, Light, et al., 2007; Perovich, Nghiem, et al., 2007). While the spring melt transitioning earlier has stronger impact than a delayed freeze, the additional cumulative solar energy absorbed for each day of later freeze is approximately 1.5 MJ m^{-2} day^{-1} (Perovich, Light, et al., 2007). Given the importance of albedo transitions over Arctic sea ice, the monitoring and detection of sea ice phenological events (e.g. melt onset, melt duration, water clear of ice, freeze onset and ice cover duration) is important for quantifying the role of sea ice in the Arctic energy budget and hence understanding impacts on the global climate system.

Microwave remotely sensed data are widely utilized for the detection of sea ice phenological events as they provide information regardless of polar darkness and extensive cloud cover. Algorithms applied to several generations of satellite passive microwave measurements (i.e. Scanning Multichannel Microwave Radiometer (SMMR), Special Sensor Microwave/Image (SSM/I) and Advanced Microwave Scanning

* Corresponding author. Tel.: +1 416 739 4385.
E-mail addresses: Laura.Brown@ec.gc.ca (L.C. Brown), Stephen.Howell@ec.gc.ca (S.E.L. Howell), mortin@misu.su.se (J. Mortin), Chris.Derksen@ec.gc.ca (C. Derksen).

http://dx.doi.org/10.1016/j.rse.2014.02.012

Radiometer for the Earth Observing System (AMSR-E)) are able to estimate melt onset and freeze onset over the Arctic (e.g. Belchansky, Douglas, & Platonov, 2004; Drobot & Anderson, 2001; Markus et al., 2009; Smith, 1998). Active microwave algorithms, specifically applied to QuikSCAT, have also been widely utilized for estimating melt onset, freeze onset and water clear of sea ice (e.g. Howell, Derksen, & Tivy, 2010; Howell, Tivy, Yackel, Else, & Duguay, 2008; Mortin, Schrøder, Walløe Hansen, Holt, & McDonald, 2012; Mortin et al., 2014; Wang et al., 2011). Active microwave algorithms using synthetic aperture radar (SAR) have also been used for high resolution retrieval of melt and freeze events (e.g. Kwok, Cunningham, & Nghiem, 2003, Winebrenner, Holt, & Nelson, 1996; Winebrenner, Nelson, Colony, & West, 1994; Yackel, Barber, & Papakyriakou, 2001). Regardless of the approach, microwave datasets all rely on a single sensor and, as a result, suffer from inherent wavelength specific uncertainties. Passive microwave measurements are at coarse spatial resolution (25 km), which leads to problems near coastal areas, and a lack of sensitivity to small leads and polynyas. QuikSCAT SIR data offer a spatial resolution improvement (4.45 km) over passive microwave derived estimates but the sensitivity to surface scattering leads to uncertainties during transient weather events (Howell et al., 2010; Yu, Clausi, & Howell, 2009). SAR estimates provide the highest spatial resolution (i.e. 100 m) but the moderate temporal resolution combined with a narrow swath width limits their application to specific regions as opposed to the entire pan-Arctic domain. To mitigate these single sensor problems the ideal approach for estimating sea ice phenology parameters is from a combination of sensors.

The Interactive Multisensor Snow and Ice Mapping System (IMS) utilizes a variety of multi-sourced datasets such as passive microwave, visible imagery, operational ice charts and other ancillary data (Helfrich, McNamara, Ramsay, Baldwin, & Kasheta, 2007; Ramsay, 1998). IMS data has been used primarily for snow applications (e.g. Chen et al., 2012; Derksen & Brown, 2012; Scott, Buehner, Caya, & Carrieres, 2013) and has also been shown to be an effective product for lake ice phenology studies (e.g. Brown & Duguay, 2012; Duguay, Brown, Kang, & Kheyrollah Pour, 2011, 2013; Kang, Duguay, & Howell, 2012). Compared to snow and lake ice applications, IMS applied to sea ice has received little attention as of yet. Recently, IMS has been used as a validation product for an ice concentration algorithm (Scott et al., 2013), and is being used to produce a daily sea ice extent product: the Multisensor Analyzed Sea Ice Extent — Northern Hemisphere (MASIE-NH; http://nsidc.org/data/masie/masie_plots.html) product.

The IMS product has not been used for monitoring ice phenology or for the creation of new sea ice phenology datasets. This paper provides the first evaluation of two newly derived datasets from IMS: a 'first open water' dataset (the detection of the ice to open water transition) and a freeze onset dataset (the detection of the open water to ice transition), by comparing them with previously established datasets. Second, we combine IMS first open water and freeze onset datasets with existing passive microwave products (SSM/I derived melt onset) for the creation of two new sea ice phenology datasets: melt duration to open water (duration from melt onset to open water), and FYI cover duration (spanning freeze onset until open water the following year), both of which have not been previously produced and provide a new perspective on sea ice phenology of particular relevance to the current era of largely seasonal ice cover.

2. Data and methods

A summary of all pre-existing data products used for comparison with IMS is presented in Table 1 and a diagram of which products were compared for each transitional event is shown in Fig. 1 (which also highlights the new IMS-based datasets). To avoid confusion between algorithm names and sensor names, an acronym is assigned to each dataset for clarity (Table 1). The temporal availability of each dataset varies, so 2004–2008 were used for comparison, as all of the products were available during these years. New spatial datasets are presented for the time span of the IMS 4 km product: 2004–present, and 24 km product: 1997–present. The subsequent sections detail the data products used, starting with IMS, and followed by the comparison data sets organized by transitional parameter (melt and freeze onset, open water detection) as well as the ancillary data used.

For consistency while comparing between datasets the following terminology will be used. 'Melt onset' is defined as the beginning of the melt of the snow on top of the sea ice (detected by SSM/I). The first occurrence of open water detected for a given pixel will be referred to as 'first open water' (detected using multiple datasets and analogous to 'water clear of sea ice' used in Howell et al., 2010). This could be a lead opening early in the season (which could subsequently refreeze), or open water that remains for the melt season. 'Continuous open water' is defined as the last change from ice to water for a given pixel signaling ice-free conditions for the remainder of the melt season (detected using IMS). For the freeze-up season, 'freeze onset' is defined as the first detection of ice for a given pixel (detected by SSM/I, QuikSCAT and IMS) while 'continuous ice cover' refers to the date of the last change from water to ice (detected using IMS). While ridging, rafting, and divergent motions (leads) are plausible with sea ice, the impact is likely minimal on these results.

2.1. IMS

The IMS product (National Ice Center, 2008, updated daily) (obtained from the National Snow and Ice Data Center (NSIDC), http://nsidc.org/data/g02156, see Table 1) provides discrete values for land, snow covered land, water and ice, and is subjectively produced by analysts at both the 4 km (2004–present) and 24 km (1997–present) resolutions on a daily basis. Data sources available to the analysts have evolved since the beginning of IMS production, and include a combination of satellite imagery: visible and infrared (e.g. Polar and Geostationary Operational Environmental Satellites (POES/GOES)) as well as passive microwave (SSMI/I and AMSR-E, when available) and other ancillary data, including a weekly sea ice analysis from the National Ice Center

Table 1
Summary of the data sources used.

Data product	Acronym	Resolution	Data source
Interactive Multisensor Snow and Ice Mapping System	IMS	4 km, 24 km	National Snow and Ice Data Center (NSIDC)
Scatterometer Image Reconstruction (SIR) SeaWinds/QuikSCAT backscatter (σ°). Algorithms: Howell et al. (2010) (transition to open water)/Mortin et al. (2012) (freeze onset)	QuikSCAT	4.45 km	Brigham Young University (BYU)
Advanced Microwave Scanning Radiometer for the Earth Observing System brightness temperature (T_B) measurements. Algorithm: Howell et al. (2010) (transition to open water)	AMSR-E	8.9 km	Brigham Young University (BYU)
Melt/Freeze Onset from the Scanning Multichannel Microwave Radiometer and Special Sensor Microwave/Image. Algorithm: Markus et al. (2009)	SSM/I	25 km	NASA Goddard
Sea Ice Concentrations from Nimbus-7 SMMR and DMSP SSM/I-SSMIS Passive Microwave Data. Algorithm: Cavalieri et al. (2008)	NASATeam	25 km	National Snow and Ice Data Center (NSIDC)
RADARSAT ScanSAR imagery	RADARSAT	100 m	Canadian Ice Service (CIS)/Alaska Satellite Facility (ASF)
Sea Ice Index	Sea Ice Index	NA	National Snow and Ice Data Center (NSIDC)

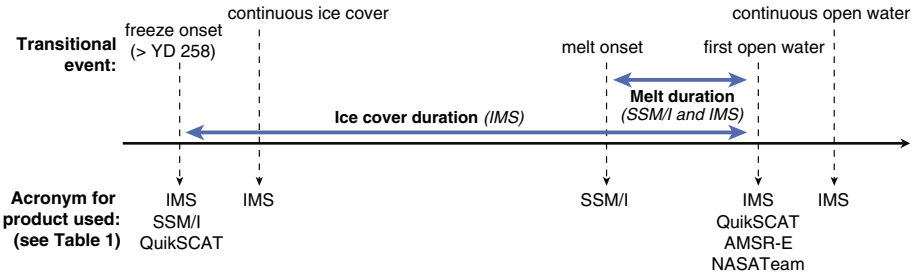

Fig. 1. Schematic time series identifying the different transitional parameters and the instruments and algorithms used. New datasets (ice cover duration and melt duration) indicated in bold.

(Chen et al., 2012, Helfrich et al., 2007; NSIDC, 2011; Ramsay, 1998). For determining sea ice presence, analysts refer first to visible imagery when not obstructed by clouds, followed by passive microwave data and National Ice Center (NIC) weekly sea ice analysis product, depending on the time of year and the resolution and data latency (NSIDC, 2011).

A day-to-day comparison was used to detect the transition from ice to water (and vice versa) for each pixel (following the same procedure developed for lake ice and described in Brown & Duguay, 2012). Two dates were extracted from the IMS product related to melt: 1) the first change from ice to water as the first occurrence of open water, and 2) the last change from ice to water signaling continuous open water for the remainder of the season. Conversely, for freeze, the first date of ice formation (freeze onset) and the final date of ice formation (continuous ice cover) were extracted. The IMS product can identify any change from water to ice (or ice to water) and can therefore be used to determine the first occurrence of open water, leads opening and closing throughout the ice covered season, as well as the final water clear of ice. The IMS product cannot be used to detect initial melt onset (wet snow over ice) to which the microwave measurements are highly sensitive (as described in Subsection 2.2).

2.2. Melt and freeze onset detection

2.2.1. SSM/I

Melt onset and freeze onset dates from the SSM/I data (obtained through NASA Goddard, see Table 1) were obtained using the passive microwave algorithm fully described by Markus et al. (2009). Briefly,

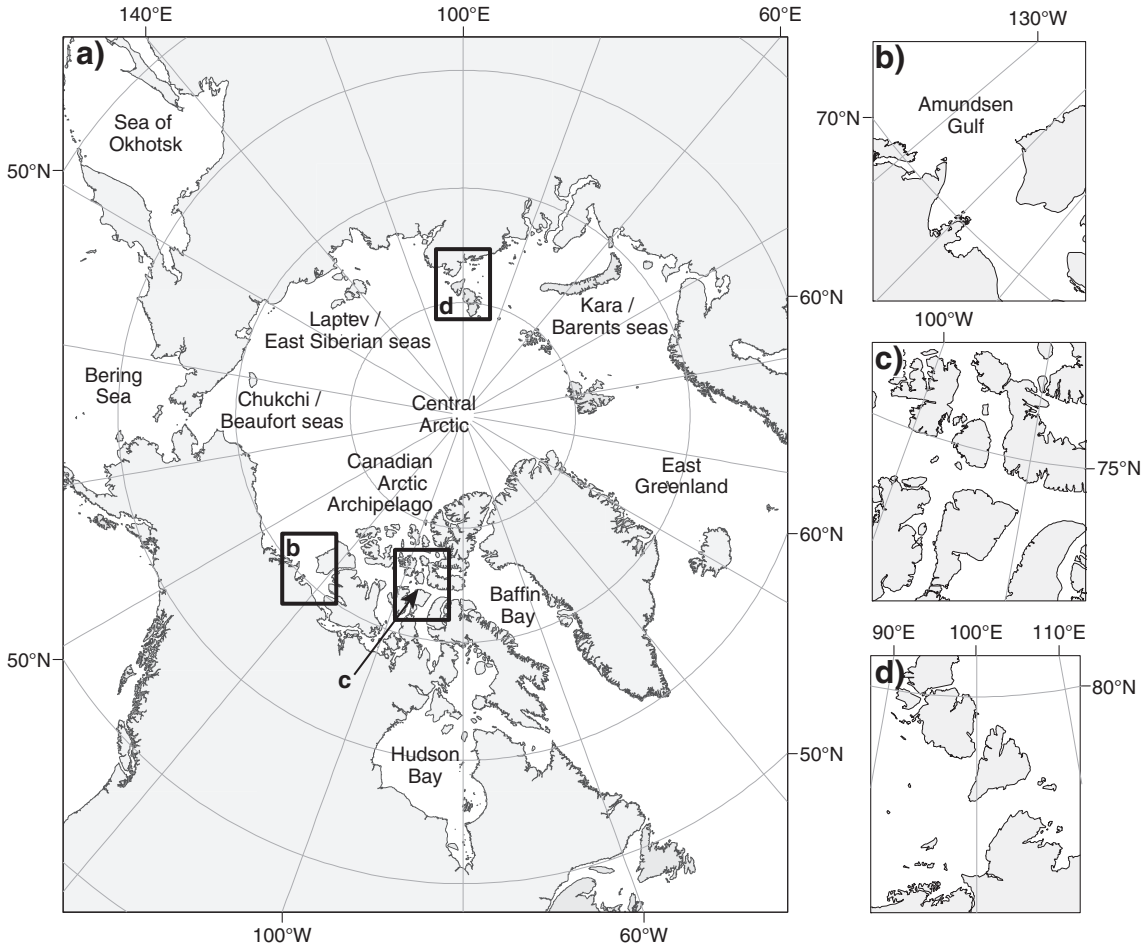

Fig. 2. a) General regions in the pan-Arctic seas and the three focus areas examined in this study: b) Amundsen Gulf region; c) Central Canadian Arctic Archipelago and d) Severnaya Zemlya Archipelago.

this method derives several indicators of melt onset and freeze onset inherent in the microwave measurements due to the strong difference in dielectrics between dry and wet snow. This approach builds on the strength of multiple indicators as they are each sensitive to different features of melt or freeze events and the agreement of these different indicators is utilized. The strength of the melt onset or freeze onset signal is determined by summing the normalized magnitude for each indicator. The day with the greatest sum is the first choice for the melt (freeze) onset day. For this study, 'early melt (freeze) onset' as defined by Markus et al. (2009) is identified as the day of the first occurrence of melt (freeze). Freeze dates prior to September 15 (the defined start of the freeze season used in this study) were excluded as these tend to represent freeze over regions of MYI rather than FYI ice formation, for comparison to the FYI formation detected by IMS.

2.2.2. QuikSCAT

Freeze onset dates from QuikSCAT SIR (obtained from the NASA sponsored Scatterometer Climate Record Pathfinder at Brigham Young University, http://www.scp.byu.edu/data.html, see Table 1), were determined using the approach described by Mortin et al. (2012). The methodology detects sharp changes, or edges, in time series of QuikSCAT backscatter (σ°) typically corresponding to major melt or freeze events at the surface associated with changes in the dielectrics when the liquid water content changes (Barber, Papakyriakou, Ledrew, & Shokr, 1995; Gogineni et al., 1992; Stiles & Ulaby, 1980). However, there are processes that introduce noise in the signal, such as sea ice dynamics. To mitigate the influence of these processes, the algorithm is iterated twice. First, estimates of the transition dates are retrieved by finding edges in the signal at different temporal scales (1–30 days). Second, the climatology of these dates is used to choose the edge most likely corresponding to major melt-freeze events at the surface, rather than other processes, such as sea ice dynamics. This iteration significantly improves spatial inconsistencies in transition dates (see Fig. 6 by Mortin et al. (2012)). The algorithm also provides an estimate of the sea ice cover from QuikSCAT measurements, following Haarpaintner, Tonboe, Long, and Van Woert (2004), with criteria giving a conservative sea ice cover estimate. For example, the algorithm estimates Hudson Bay, Bering Sea, and parts of Baffin Bay as being ice free (see Fig. 10 by Mortin et al. (2012)). Using this algorithm, Mortin et al. (2012) retrieved melt and freeze onset over land and sea ice across the Arctic Ocean during 1999–2009 (the full lifetime of QuikSCAT). In this study, we utilize the freeze onset in the marginal seas (as their product also covers the Arctic multiyear ice pack where melt to open water typically does not occur on a large scale) from 2004 to 2008. Similar to the passive microwave, data points with freeze prior to September 15 were excluded.

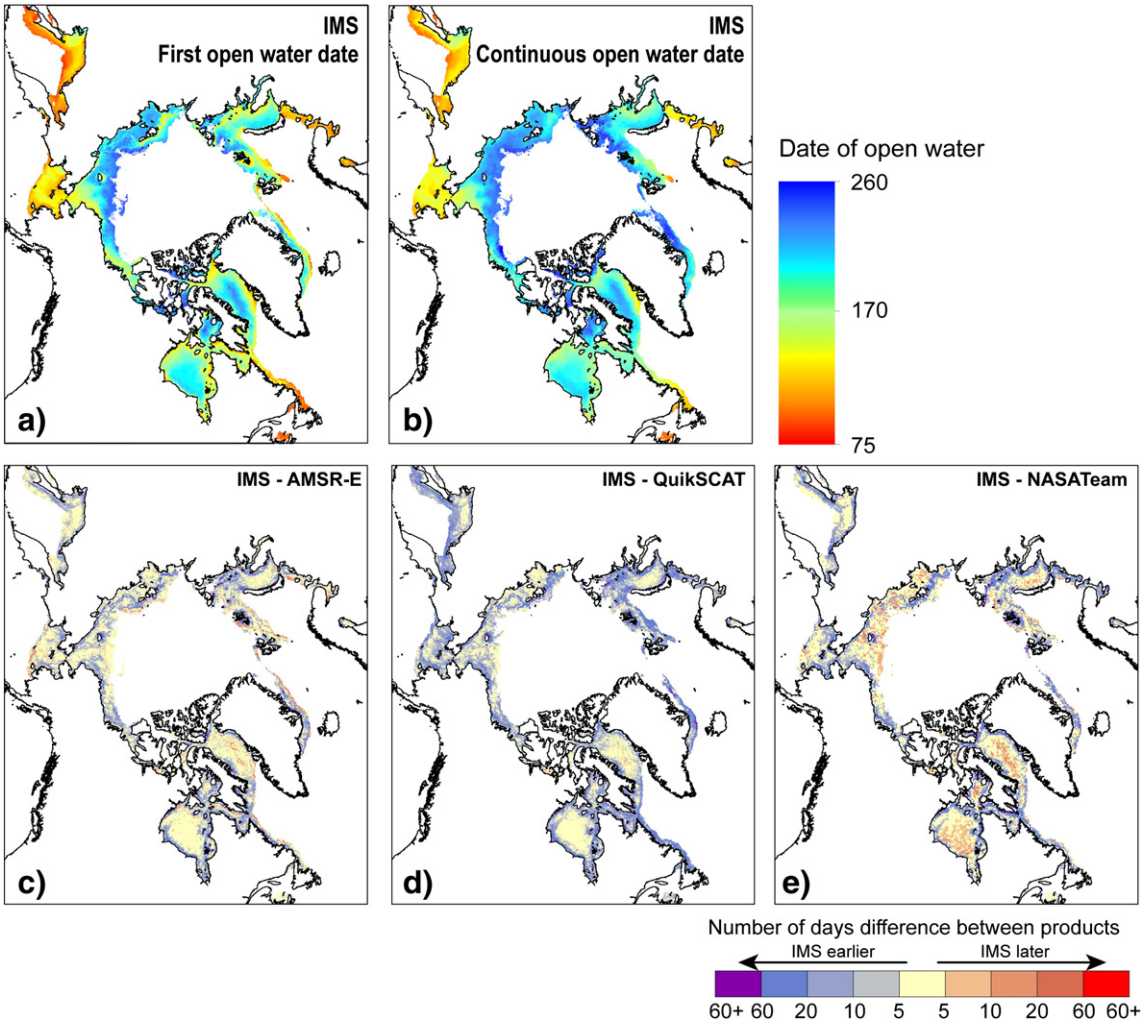

Fig. 3. Comparison of the mean (2004–2008) first open water date from IMS (a) and continuous open water date from IMS(b), and the difference in number of days between IMS and c) AMRS-E, d) QuikSCAT and e) NASATeam datasets, for mean (2004–2008) first open water date. Only pixels with open water identified in all five years are compared.

Table 2
Pan-Arctic mean dates and standard deviation (days) for first open water.

	IMS		AMSR-E		QuikSCAT		NASATeam	
	Mean	SD	Mean	SD	Mean	SD	Mean	SD
2004	172 (Jun. 20)	53.2	173 (Jun. 21)	55.6	178 (Jun. 26)	48.4	173 (Jun. 21)	51.5
2005	171 (Jun. 20)	52.0	176 (Jun. 25)	51.7	179 (Jun. 28)	45.1	176 (Jun. 25)	48.0
2006	165 (Jun. 14)	54.5	173 (Jun. 22)	53.2	177 (Jun. 26)	46.0	173 (Jun. 22)	48.9
2007	168 (Jun. 17)	52.2	176 (Jun. 25)	51.8	181 (Jun. 30)	45.1	177 (Jun. 26)	47.3
2008	173 (Jun. 21)	51.4	176 (Jun. 24)	52.4	179 (Jun. 27)	47.2	177 (Jun. 25)	48.6
5 year mean	170	53	175	53	179	46	175	49

2.3. Open water detection

2.3.1. QuikSCAT

QuikSCAT was also used to determine first open water estimates, which were obtained using the approach described by Howell et al. (2010). The approach only detects the first appearance of open water and any potential refill of ice is not accounted for. The algorithm tracks the evolution of the QuikSCAT σ° obtained at both horizontal (σ°_H) and vertical (σ°_V) polarizations. Over an initially sea ice covered ocean, an estimate of the first date of open water is detected by a simultaneous decrease in thresholds for both polarizations. The thresholds are only applicable to calm wind conditions and as a result, open water detection may be late during rapid ice clearing events (with concurrent high wind speeds) or in the marginal ice zones.

2.3.2. AMSR-E

AMSR-E data (obtained from the NASA sponsored Scatterometer Climate Record Pathfinder at Brigham Young University, http://www.scp.byu.edu/data.html, see Table 1) first open water estimates where obtained using the threshold approach described by Howell et al. (2010). Similar to the estimates obtained from QuikSCAT, this approach only detects the first appearance of open water so potential refill of ice is not accounted for. The ASMR-E first open water detection algorithm uses the temporal evolution of the brightness temperature (T_B) polarization ratio at 18.7 GHz (PR18). Unlike σ°, T_B is influenced by the physical temperature of the surface and emissivity.

2.3.3. Passive microwave ice concentrations

Water clear of sea ice estimates were also determined when the sea ice concentration retrieved by the NASATeam algorithm (Cavalieri, Parkinson, Gloersen, & Zwally, 2008) reached 0 tenths (following Howell et al., 2010) to represent ice free conditions. This ice concentration dataset is a long term time series (1978–present) based on T_B data from SSMR and SSM/I passive microwave sensors, at a 25 km resolution. For a detailed description of this dataset refer to http://nsidc.org/data/docs/daac/nsidc0051_gsfc_seaice.gd.html.

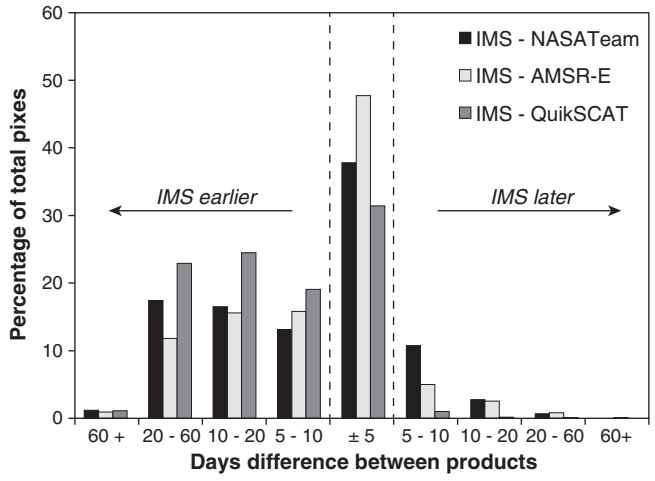

Fig. 4. Percent difference between IMS and each compared dataset for mean (2004–2008) first open water date in overlapping areas.

2.4. Ancillary

2.4.1. RADARSAT

RADARSAT-1 ScanSAR imagery (100 m resolution, see Table 1) was acquired from the Alaska Satellite Facility and Canadian Ice Service to serve as an independent validation data source for inter-product comparison. RADARSAT-1 ScanSAR images consist of a series of merged beams (Wide Beams 1, 2, and 3 and Standard Beams 5, 6 and 7) that are aggregated to produce a 460 km swath. RADARSAT data were obtained for three focus regions on selected days from 2007: 1) Amundsen Gulf region (Fig. 2b) which is typical of a region with complicated ice patterns due to lead formations; 2) the Central Canadian Arctic Archipelago (Fig. 2c) covering the northern route of the Canadian Northwest Passage, and 3) the Severnaya Zemlya Archipelago (Fig. 2d) representing one of the routes of the Northern Sea Route.

2.4.2. Sea Ice Index

The National Snow and Ice Data Center (NSIDC) Sea Ice Index (NSIDC, 2008, updated 2013) was used to normalize the maximum extent of the sea ice edge between all products, by setting the extent boundaries to the mean March sea ice extent from the NSIDC Sea Ice Index. Briefly, this product is a combination of near-Real-Time DMSP SSM/I-SSMIS Daily Polar Gridded Sea Ice Concentrations and historical Sea Ice Concentrations from Nimbus-7 SMMR and DMSP SSM/I-SSMIS Passive Microwave Data (Fetterer, Knowles, Meier, & Savoie, 2002) used to create daily and monthly extents of the sea ice (using the NASA Team algorithm). For the monthly extent data, the ice edge is defined by a mean ice concentration of 15%. See the product documentation from NSIDC for a more detailed description: http://nsidc.org/data/docs/noaa/g02135_seaice_index/index.html.

3. IMS comparison

The following sections present a comparison of 1) our first open water estimates obtained from IMS with previously developed datasets derived from QuikSCAT, ASMR-E, and SSM/I (NASATeam) and 2) freeze onset estimates obtained from IMS, QuikSCAT and SSM/I. It should be reiterated that IMS relies on variable sources of input data (which is not tracked in the form of metadata), and so is not completely independent of the evaluation data sets. For instance, it is likely that passive microwave data was used by the analysts in some instances. The RADARSAT-1 data is a completely independent source for comparison.

3.1. First open water detection

Spatially, the mean state of all datasets follows a similar pattern (Fig. 3, IMS shown) with the earliest first open water dates occurring at the maximum ice extent in March (YD 75) and the latest dates near the ice minimum extent in mid-September (YD 260). For all datasets,

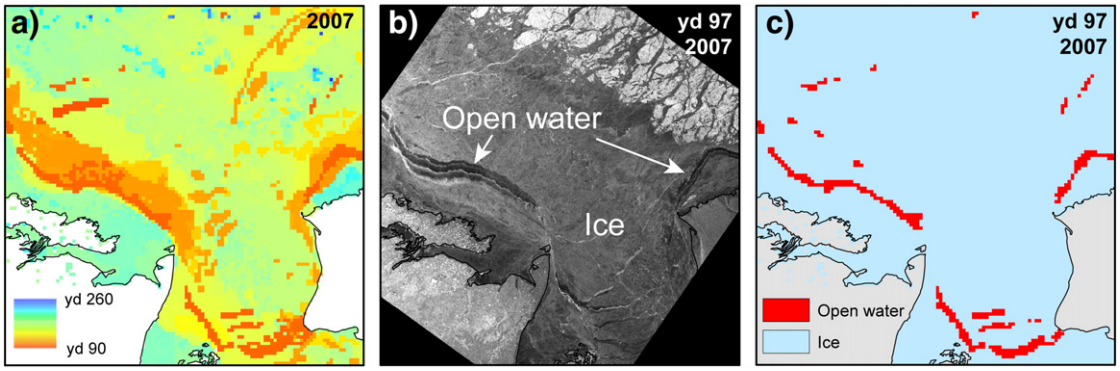

Fig. 5. (a) IMS first open water dates from the Amundsen Gulf region (Fig. 2b); (b) RADARSAT imagery; and (c) IMS raw data from YD 97 (April 7) 2007, showing an example of the lead detection possible using IMS.

the largest differences occur primarily at the FYI and MYI boundary in the central Arctic Ocean as well as along the coastlines (Fig. 3 c, d, e). All compared datasets cover an identical spatial domain, and the IMS dataset was resampled to the lower of the two resolutions being compared (4.45 km for QuikSCAT, 8.9 km for AMSR-E, and 25 km for NASATeam).

For all years, the mean first open water date is detected initially by IMS (YD 170 (Jun. 19) ± 53), followed by AMSR-E (YD 175 (Jun. 24) ± 53), NASATeam (YD 175 (Jun. 24) ± 49) and then QuikSCAT (YD 175 (Jun. 28) ± 46) (Table 2). Only pixels with open water identified in all five years are compared. The standard deviation for all datasets is similar and ranges from 46 to 53 days, a reflection of the large variability with respect to sea ice clearing dates from the southern to northern regions (Table 2).

The AMSR-E first open water dataset has the largest percentage of pixels in agreement (defined as ±5 days) with IMS at 48% (Fig. 4). Of the remaining AMSR-E pixels not within ±5 days of IMS, 8% were earlier than IMS first open water dates (IMS had later dates) and 44% were later than IMS first open water dates (IMS had earlier dates) (Fig. 4). Only 31% of the pixels from the QuikSCAT first open water dataset were within ±5 days of IMS (Fig. 4). Compared to IMS, QuikSCAT pixels were also heavily skewed to towards later first open water dates (IMS had earlier dates) (65%) and only 1% of the pixels had earlier first open water dates than IMS. Comparing IMS to the NASATeam open water dates finds 38% of the total pixels within ±5 day agreement with IMS (Fig. 4). Of the pixels not within ±5 days, 14% detected earlier first open water dates than IMS and 48% of pixels were later than IMS.

With respect to coastal areas, IMS typically detected earlier first open water dates compared to the other datasets but agreement improves with distance away from the coast (Fig. 3c,d,e). Comparing NASATeam and IMS (Fig. 3e), not only can the open water be detected closer to the shoreline with IMS due to resolution, but also some coastal contamination (i.e. mixed land–sea ice pixels) can remain in the NASATeam data even after reduction techniques are applied to the raw data (post-processing), resulting in falsely identified ice

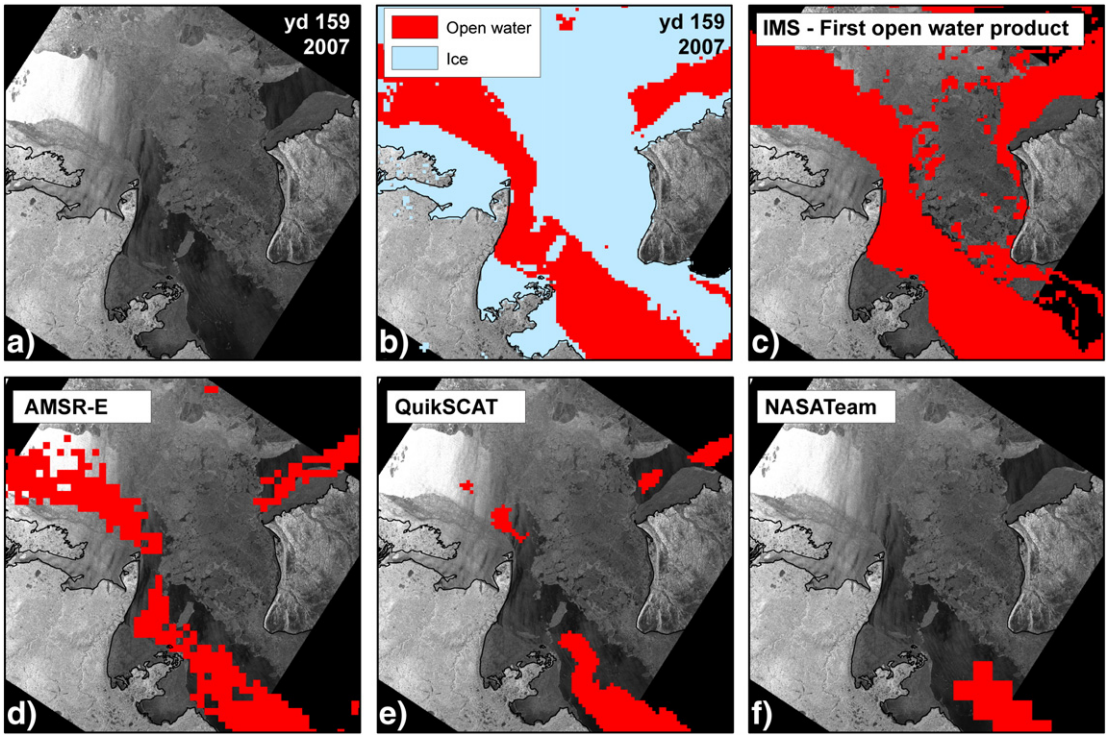

Fig. 6. Open water as of YD 159 (June 8), 2007 in the Amundsen Gulf region (see Fig. 2b) as identified by each dataset: a) RADARSAT, b) IMS raw data categories, c) IMS first open water dataset, d) AMSR-E, e) QuikSCAT and f) NASATeam.

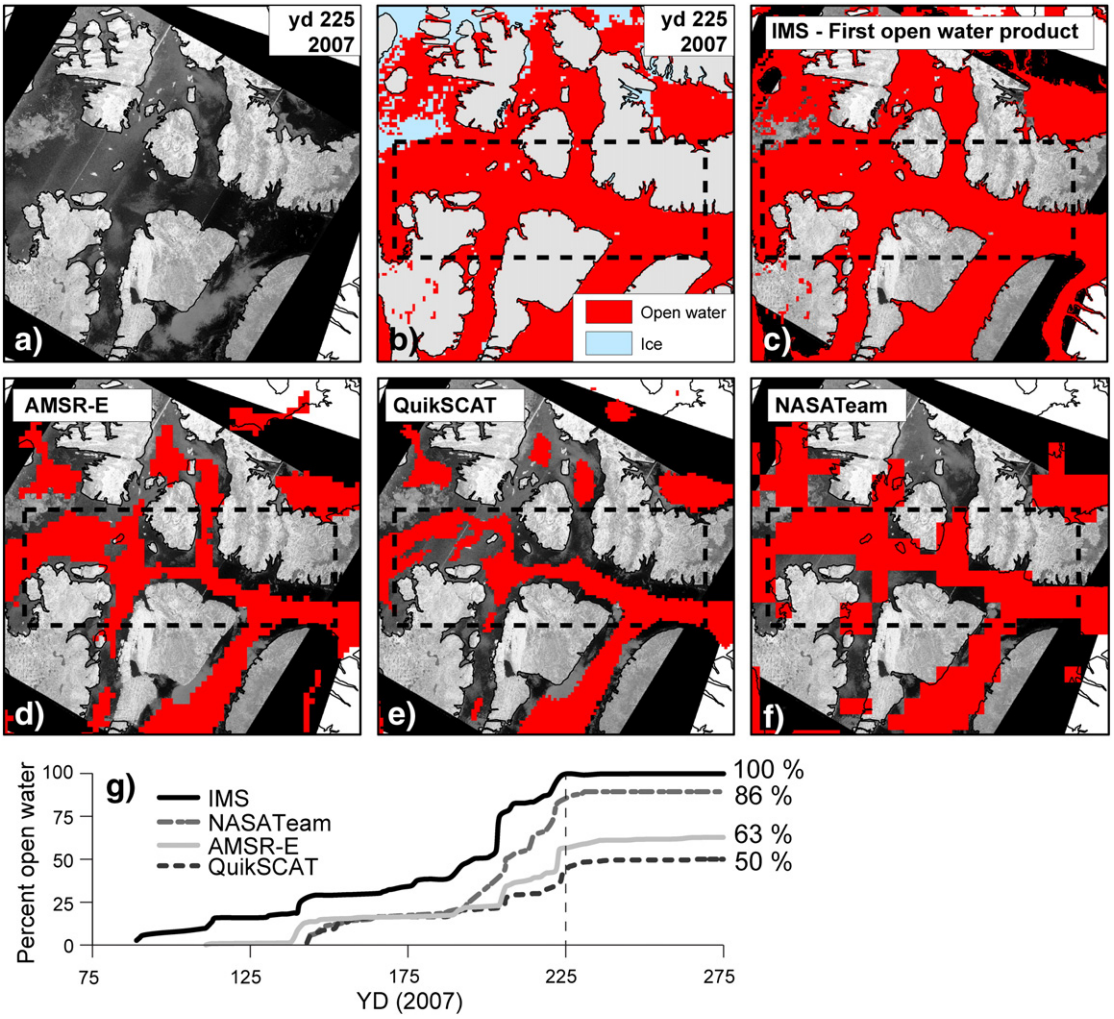

Fig. 7. Open water as of YD 225 (August 13), 2007 in the North West passage (see Fig. 2c) region as identified by each dataset: a) RADARSAT, b) IMS raw data categories, c) IMS first open water dataset, d) AMSR-E, e) QuikSCAT and f) NASATeam; and g) the time series of percent open water in the bounding box (dashed line in maps) indicated in b–f, with the final end of season percentage of possible open water identified. The vertical dashed line in g marks the date shown in the maps.

concentrations along the shorelines (NSDIC, 2006). Comparing AMSR-E and IMS (Fig. 3d) shows less difference in the coastal regions, presumably due to the finer resolution of AMSR-E (8.9 km). QuikSCAT however, shows more extensive regions near the coastal areas where open water is detected later than IMS (Fig. 3d). While the QuikSCAT data used in this study was reconstructed to a grid resolution of 4.45 km (Long, Hardin, & Whitling, 1993), the effective resolution is 8–10 km (Long & Hicks, 2005), which could result in some coastal contamination. However, the late detection of open water with QuikSCAT could also be attributed to weather influences, as the transition from ice to open water is often the result of wind, which in turn results in backscatter values similar to those over land due to wind roughening of the surface.

Large areas of seasonal FYI (e.g. Hudson Bay and Baffin Bay) show IMS with later first open water dates compared to NASATeam (Fig. 3e). These differences are greatest in 2004 and 2008 (not shown) and are likely attributable to the native resolution of the products. While both are gridded to 25 km for comparison, the original SSM/I passive microwave data used to create the 25 km sea ice concentration data can have footprints ranging up to 70 × 45 km (at 19.3 GHz), missing the regions of later melt visible in the finer 4 km IMS. Earlier first open water dates from NASATeam could also be attributed in part to the presence of the melt ponds on top of the ice, which is a widely known problem with ice concentration retrieval algorithms (Agnew & Howell, 2003; Cavalieri, Parkinson, Gloersen, Comiso, & Zwally, 1999). The higher agreement between AMSR-E and IMS when compared against NASATeam and IMS is likely attributable to the higher spatial resolution of AMRS-E, though the different algorithms used to produce each dataset could also be a factor. Conversely, the better agreement with AMSR-E and IMS compared to QuikSCAT and IMS is likely due to the reduced sensitivity to transient weather events that can affect QuikSCAT (Howell et al., 2010; Yu et al., 2009).

Fig. 5 provides a good example of the ability of IMS to identify leads opening and subsequently closing early in the season, which is a frequent occurrence in the Amundsen Gulf area (Fig. 2b). IMS detects open water dates circa YD 90 (March 31) (Fig. 5a) in the area where leads are clearly apparent on a coincident RADARSAT image for YD 97 (April 7) (Fig. 5b) and the corresponding IMS data from the same day

Table 3
Percent greater extent open water detected by IMS in the Barrow Strait at end of the melt season compared to AMSR-E, QuikSCAT and NASATeam products.

	Percent greater extent of open water detected by IMS compared to:		
	AMSR-E	QuikSCAT	NASATeam
2004	27.5	45.7	35.6
2005	33.7	64.7	5.3
2006	37.3	52.5	20.0
2007	37.0	49.8	10.5
2008	37.8	51.4	14.1
5 year mean	34.6	52.8	17.1

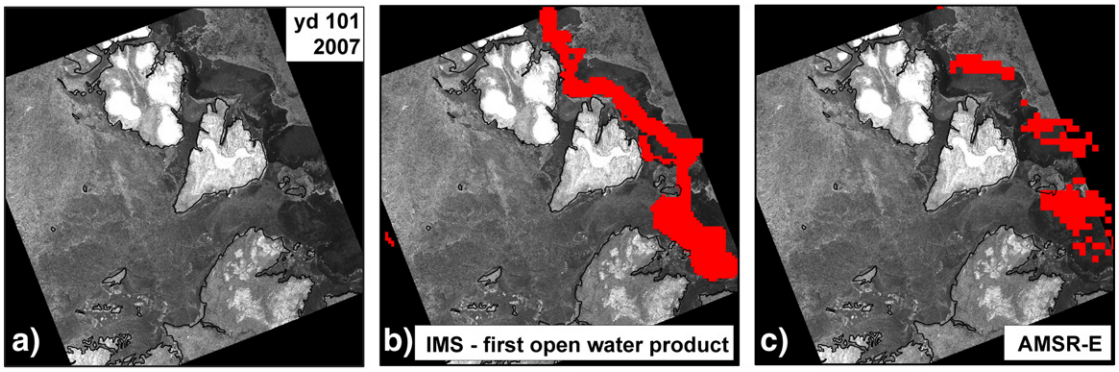

Fig. 8. Open water as of YD 101 (April 11), 2007 in the Vilkitsky Strait/Severnaya Zemlya Archipelago (see Fig. 2d) as identified by each dataset: a) RADARSAT, b) IMS first open water dataset and c) AMSR-E.

(Fig. 5c). The ability of IMS to identify the first occurrence of open water better than the other datasets is even more apparent as the melt season evolves. For example, Fig. 6 displays the first open water dates by YD 159 (June 8) for each dataset overlaid on RADARSAT images for the same day. IMS shows the most open water, including some small areas that were likely open earlier as leads but on YD 159 were no longer open. IMS on YD 159 is clearly in good agreement with the RADARSAT imagery for open water on that date, while the other datasets all drastically underestimate the amount of open water present by that date.

In addition to improved characterization of the timing of open water, the IMS dataset is able to better capture the extent of the transition from ice to open water (first open water) than the other datasets in narrow channels and straits, which could have operational implications for IMS datasets with respect to marine navigation. For example, while all four datasets do show the opening of the northern route of the Northwest Passage (Fig. 2c) by YD 225 (Aug. 13) in 2007, only IMS shows the full extent of the open water (Fig. 7). Using the boundary indicated on Fig. 7 (focussed on Barrow Strait) the percentage of open water throughout the melt season each year was determined by tallying the total number of pixels (hence determining the area) with open water each day until the end of the melt season was reached (Fig. 7g, 2007 shown). IMS identified the greatest percentage of open water from 2004 to 2008, followed by NASATeam, ASMR-E, and QuikSCAT, which consistently identified the least percentage of open water (Table 3). On average (2004–2008), IMS identified 53% more open water than QuikSCAT, 35% more open water than AMSR-E and 17% more open water than NASATeam in the Barrow Strait region of the Northwest Passage (Table 3) showing that that the microwave-only algorithms are systematically underestimating the area of open water. Further highlighting the utility of IMS, looking at the Northern Sea Route on the Eurasian side of the Arctic Ocean (Fig. 2d), IMS shows the ice opening along the eastern side of the Severnaya Zemlya Archipelago (Fig. 8). The second best estimate came from AMSR-E, which only detected small openings (Fig. 8). No open water dates were detected by NASATeam or QuikSCAT (not shown).

Although the product comparison in this study focuses on 2004–2008, an interesting situation is presented for the 2012 season, where exceptional melt occurred. Looking at daily comparison of pan-Arctic ice extent for 3 select days during the 2012 melt season highlights the regions where the NASATeam (daily ice concentrations, shown spatially where concentration is 15% or greater) and IMS are not in agreement (Fig. 9). Compared to IMS, the NASATeam dataset tends to underestimate the presence of open water by September in the near-shore areas, particularly the Eurasian and CAA coastal areas, and shows ice remaining in the inlets and channels surrounding the CAA where IMS shows open water (also shown in Fig. 7 where NASATeam is underestimating open water in the CAA). An example of how daily differences can exist between the two datasets occurred in August 2012 when a large atypical polar cyclone occurred over the Arctic Ocean during the first 2 weeks of August (Simmonds and Rudeva (2012)). This cyclone is thought by some to have greatly influenced the distribution of the sea ice in the region (e.g. Parkinson & Comiso, 2013). The passive microwave estimates show a large section of sea ice loss by August 10 (0.4×10^6 km^2) (evident in Fig. 9 on August 15) throughout the Chukchi/Beaufort seas (Parkinson & Comiso, 2013) that is not reflected until August 18 in the IMS data (not shown), possibly as a result of the obstructing cloud cover. As the IMS analysts would likely be relying more on visible imagery during the summer months, the first day of cloud-free data would be the first day where open water would be detected, while the passive microwave data may have

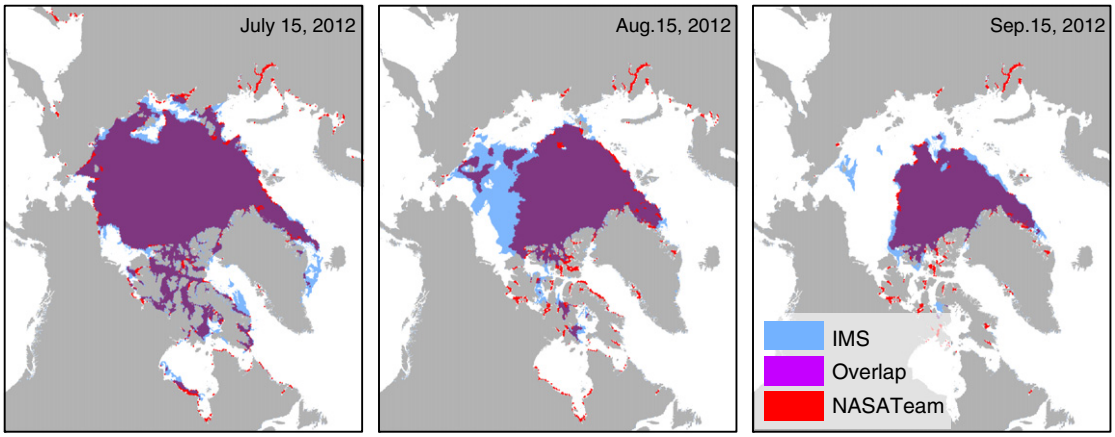

Fig. 9. Comparison of mid-month sea ice extents from IMS and NASATeam for 2012.

detected open water below the clouds. Conversely, the passive microwave data may have misidentified potential flooded or broken ice during the storm as open water. Without in situ data to confirm, no conclusions can be drawn on which sensor is more accurate.

3.2. Freeze onset

The IMS pan-Arctic freeze onset follows the typical latitudinal pattern (i.e. north to south) similar to QuikSCAT and SSM/I (Fig. 10, IMS shown). Comparing IMS and SSM/I illustrates that better agreement occurs away from the coastlines in large homogenous ocean areas (e.g. Hudson Bay) analogous to the first open water comparisons. Near the coastlines, SSM/I detected freeze onset later than IMS (Fig. 10b). This further illustrates the problem with the automated detection of phenological events near the coastline with coarse resolution microwave products.

Table 4 presents the comparison of freeze onset dates between IMS, QuikSCAT and SSM/I for all overlapping years (2004–2008). Over the study period, the freeze onset estimates from QuikSCAT were the earliest (YD 282 (Oct. 9) ±18), followed by those from SSM/I (YD 317 (Nov. 13) ±40) and then those from IMS (YD 332 (Nov. 28) ±45) (Table 4). The standard deviation for QuikSCAT dates is much lower than the others at 18 days, which can be attributed to the fact that the included freeze onset data from QuikSCAT are in regions that typically experience similar freeze dates (the QuikSCAT dataset used in this study was developed for the Arctic Ocean regions only, see Mortin et al., 2012), compared to SSM/I, which includes data outside the Arctic Ocean where freeze occurs later in the season. Additionally, only a small sample size of pixels from QuikSCAT remained when the mean date was determined, as only the coinciding areas of ice detected in all five years after the exclusion of freeze prior to YD 258 (Sept. 15) were included (see Fig. 10c).

For freeze onset, 31% of the SSM/I estimates were within ±5 days of IMS (Fig. 11). In terms of disagreement, the majority of the IMS pixels (69%) experienced a later date when compared to SSM/I with more than half of these concentrated in the 5–10 day bin. Only 15% of the QuikSCAT pixels are within ±5 days of IMS and of the remaining pixels, 1% show earlier freeze onset with IMS and the remaining 84% of the pixels show later freeze onset with IMS (with 43% of these being more than 10 days later). The average freeze dates by Mortin et al. (2012) are earlier than those from IMS because the backscatter variability from QuikSCAT during the melt season due to wind roughening of the water surface is commonly larger than the freeze-up signal indicator in the marginal seas. This causes the automated algorithm to retrieve an erroneous, early freeze-up. Because IMS uses a combined sensor approach in addition to visual assessment by analysts, it is likely to be more representative of reality than these automated approaches. For example, looking at the Amundsen Gulf (Fig. 2b) YD 299 (Oct. 26) 2007 for IMS, QuikSCAT and SSM/I (Fig. 12 a–d) freeze onset datasets and a coincident RADARSAT image with an area of open water remaining illustrates better freeze onset agreement between RADARSAT and IMS. It is important to note that as freeze onset occurs over the entire Amundsen Gulf region by YD 303(Oct. 30) (Fig. 12 e–h), problems with all datasets are still apparent. Fig. 12e shows a complete ice cover in the RADARSAT image; IMS (Fig. 12f) and QuikSCAT (Fig. 12g) still show open water; while SSM/I (Fig. 12h) shows complete ice cover.

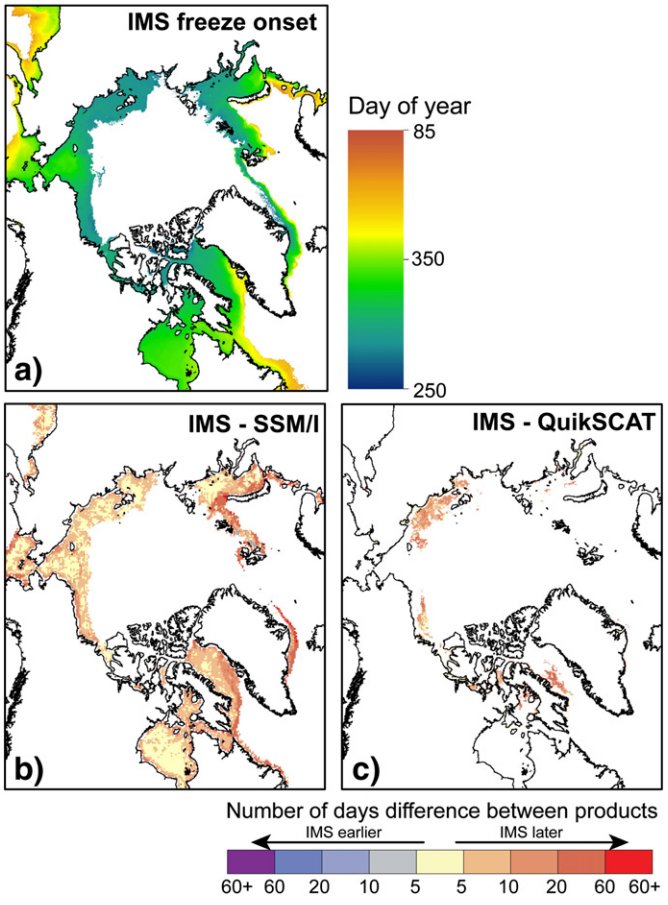

Fig. 10. Mean freeze onset maps (2004–2008) for a) IMS, and the number of days difference between d) IMS and SSM/I and e) IMS and QuikSCAT. Only pixels with open water identified in all five seasons are compared.

4. New datasets

4.1. Melt duration to open water

The Arctic melt season length over sea ice has (with some regional variability) been increasing since 1979 (e.g., Belchansky et al., 2004; Markus et al., 2009). These estimates of melt season length are typically calculated from the difference between melt onset (i.e. the initial snowmelt on top of the sea ice) and freeze onset irrespective of sea ice type (e.g. Mortin et al., 2012). The melt duration to open water (rather than to freeze onset) (MD) of freshwater ice has been previously estimated by ASMR-E and QuikSCAT (Kang et al., 2012; Howell, Brown, Kang, & Duguay, 2009) but not over sea ice. Using IMS to identify the change to open water, if present, provides a new, useful sea ice phenology dataset to examine the actual melt duration of the ice, rather than the length of the entire melt season (see Fig. 1). The dataset is created by determining the length of time from the first indication of melt onset ('early melt' from Markus et al., 2009) associated with the initial melt, through to the first detection of open water (based on IMS, resampled to 25-km pixels to match SSM/I) for overlapping areas in both datasets. Melt onset data was gridded (25 km pixels) and interpolated to the boundary of the mean March sea ice extent (NSIDC Sea Ice Index). Areas where melt onset is detected later than open water are excluded, as these areas can generally be attributed to interpolation errors near the sea ice edge where no melt was detected by SSM/I, but values from nearby pixels were used in the interpolation.

Table 4
Pan-Arctic mean dates for freeze onset.

	IMS — Freeze onset		SSM/I (EFO)		QuikSCAT	
	Mean	SD	Mean	SD	Mean	SD
2004	335 (Nov. 30)	46.0	318 (Nov. 13)	42.6	277 (Oct. 4)	18.6
2005	333 (Nov. 29)	43.1	321 (Nov. 17)	40.4	284 (Oct. 11)	18.0
2006	333 (Nov. 29)	44.3	315 (Nov. 11)	37.6	283 (Oct. 10)	18.2
2007	331 (Nov. 27)	43.9	315 (Nov. 11)	37.2	284 (Oct. 11)	18.7
2008	328 (Nov. 23)	45.7	317 (Nov. 12)	42.4	281 (Oct. 8)	17.9
Mean	332	45	317	40	282	18

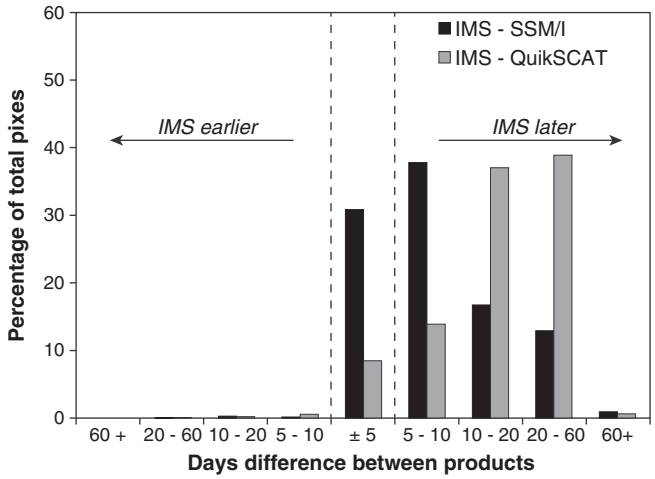

Fig. 11. Percent difference between IMS and each compared dataset for mean (2004–2008) freeze onset date in overlapping areas.

Fig. 13 shows the MD dataset from 2004 to 2012. In most cases the MD represents the melt of FYI, however some areas of MYI completely melt as well. The MD is highly variable spatially, with the shortest durations typically occurring near the same coastal regions year to year (e.g. Amundsen Gulf region, Alaska/southern Siberia, Sea of Okhotsk) as well and the southern margins of the sea ice. The eastern Siberian Sea and the southern reaches of Hudson Bay tend to have longer melt durations than other coastal areas, with some years showing long durations comparable to those found at the FYI/MYI ice margin.

The time series of mean pan-Arctic MD from 2004 to 2012 (4 km product) and from 1997 to 2012 (25 km product) is shown in Fig. 14a. The consistent, approximately two day difference in the MDs between the 4 km and 24 km IMS products is attributed to the resolution differences: the 24 km product does not capture the detail in the melt that is possible with the 4 km product, resulting in slightly later open water dates. Examining the MD from 1997 to 2012 shows slightly increasing melt durations for FYI (2 days decade^{-1}, not significant). Not only has the amount of sea ice melt throughout the pan-Arctic increased significantly over the full IMS record (Fig. 14b) (0.1×10^6 km^2 y^{-1}, $p < 0.01$), but also the mean first open water date has shifted to occur later (4 days decade^{-1}, $p < 0.05$). Increasing amounts of MYI are disintegrating during the melt season (replaced by FYI) further north in the colder regions of the Arctic and later in the melt season, which delays the overall mean open water date and contributes to the longer melt durations. While the latitudinal pattern of MDs (Fig. 14c) shows reduced MD over time in the lower latitudes (<70°N), the higher latitudes (>70°N), where the bulk of the sea ice is located, show increasingly longer MDs (with high temporal variability), driving the overall trend towards longer MDs.

The years with the greatest area of sea ice melt do not reflect the longest melt durations (cf. Fig. 14a and b). Rather, during the time span of the IMS record, extensive melt tends to happen quickly rather than prolonged over the summer season, with an exception being the record low sea ice extent of 2012. Parkinson and Comiso (2013) identify that, in contrast to previous years, the sea ice retreated faster than normal in early June 2012 but then remained comparable to previous years with large melt (2007, 2011) until early August when the melt accelerated (in part due to a large polar cyclone). After this, the decrease in sea ice extent continued at a slower rate until September 13, 2012 when the minimum was reached. Although IMS detected the large August reductions later than the passive microwave, the prolonged melt duration is still identified.

4.2. First year ice cover duration

The ice cover duration (ICD) for FYI spans from the freeze onset date in the fall until open water is reached during the melt season of the following year. ICD maps for sea ice (FYI) created from 4-km IMS data from 2004 to 2012 are shown in Fig. 15. IMS has previously been used successfully to determine ICD for lake ice (Brown & Duguay, 2012; Duguay, Brown, Kang, & Kheyrollah Pour, 2012, Duguay et al., 2013). The ICD dataset for FYI based on IMS was created by determining the number of days from freeze onset until first open water the following calendar year. Since only IMS data is used for this dataset, no sea ice edge standardization was needed and the full extent of the IMS data was used. Data presented here is the ICD to first open water, however

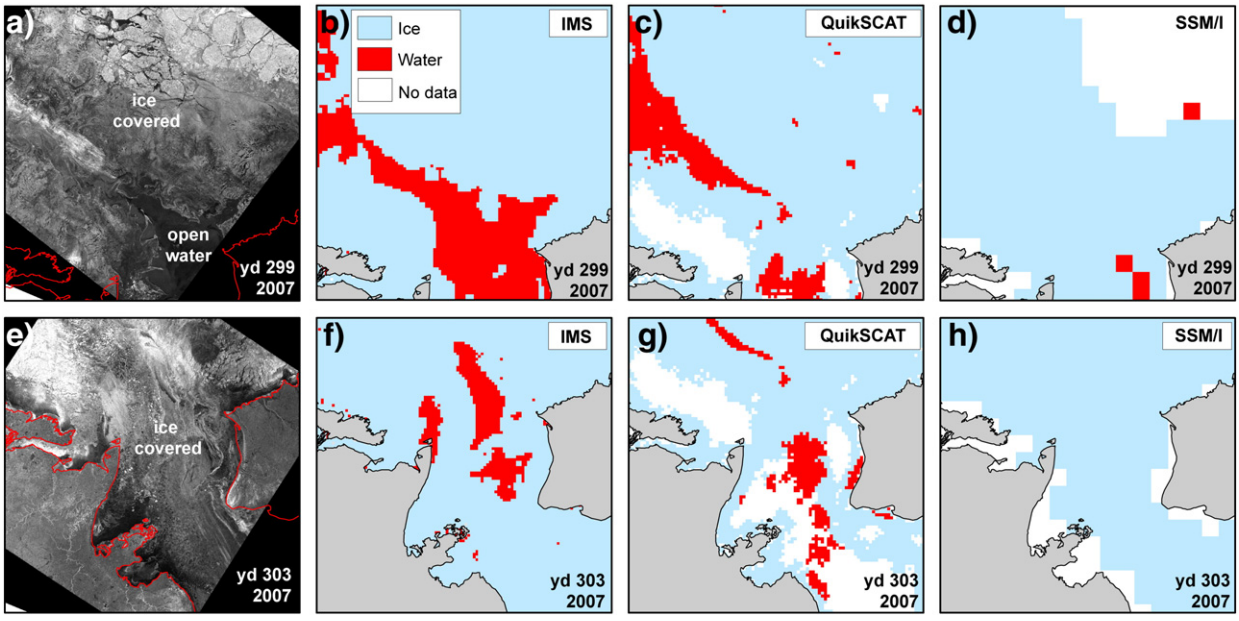

Fig. 12. Open water and ice cover as of YD 299 (October 26), 2007 in the Amundsen Gulf region as identified by: a) RADARSAT, b) IMS, c) QuikSCAT, and d) SSM/I; and on YD 303 (October 30) e) RADARSAT (ice covered), f) IMS, g) QuikSCAT, and h) SSM/I. White areas represent no data. YD 303 imagery is slightly to the south of YD 299 due to availability of RADARSAT imagery.

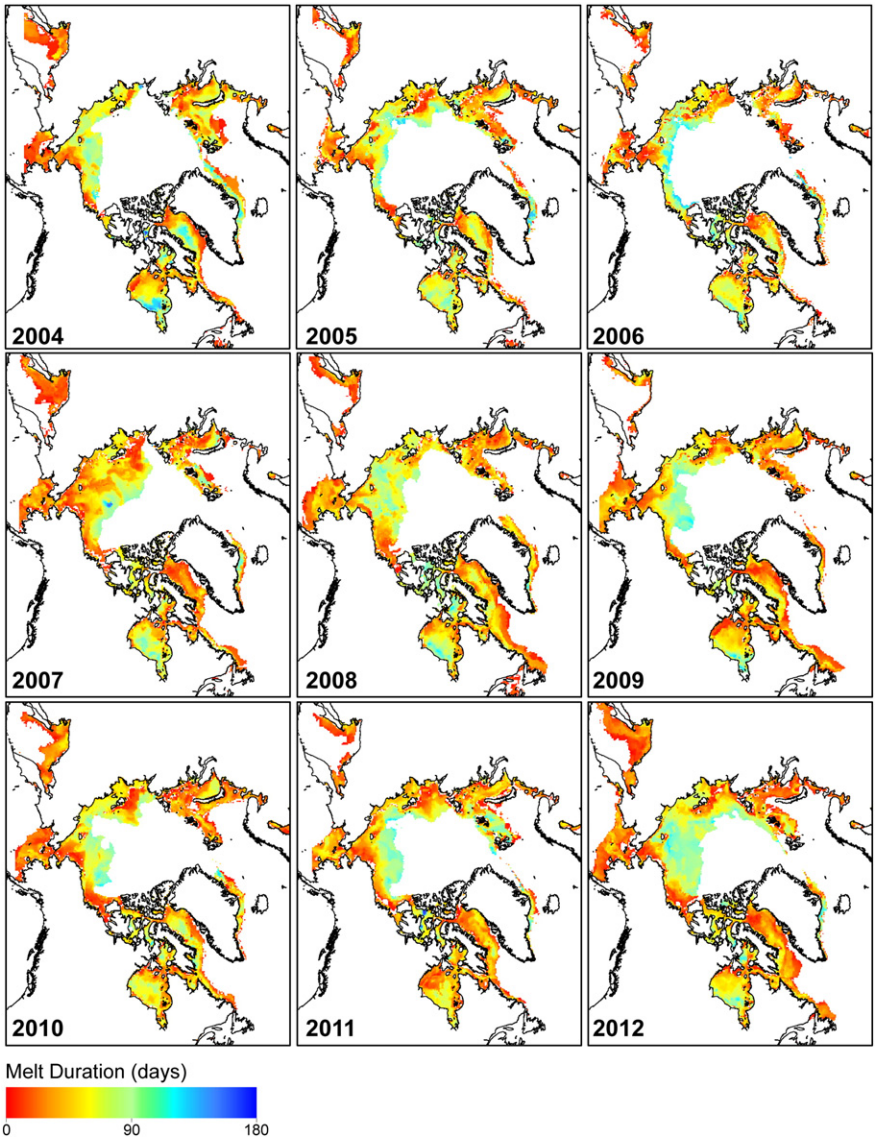

Fig. 13. Maps of melt duration to open water, i.e., from early melt onset (SSM/I) until first open water (IMS).

the ICD could also be created to the continuous open water date, which could have use for applications more focussed on navigation than climatology, particularly in regions prone to lead or polynya formation. The mean ICD for sea ice ranged from 185 to 199 days over the pan-Arctic from 2004 to 2012 (Fig. 15), but spatially the ICD can vary from as little as 1 day up to 381 days (ice that melted later than it froze the previous year, only occurring over very small areas) displaying a typical latitudinal progression from shortest to longest duration.

The time series of mean pan-Arctic ICD from 2004 to 2012 (4 km product) as well as from 1997 to 2012 (24 km product) is shown in Fig. 16a. From 1997 to 2012, earlier mean freeze onset dates (5 days decade^{-1}, $p < 0.01$) and later mean first open water dates (4 days decade^{-1}, $p < 0.05$) for the pan-Arctic result in an overall increasing trend for the mean ICD of FYI (7 days decade^{-1}, $p < 0.05$) (Fig. 16a). As with the MD, this pattern can be attributed to the larger areas of sea ice experiencing melt (and subsequent re-freeze, beginning the record of first year ICD) further into the higher latitudes (>70°N) (Fig. 16b). This newly open water then experiences freeze onset after a short open water season, effectively leading to an increase in the ICD of FYI overall. Ice dynamics could also factor in to changes in ICD of FYI, as the FYI could potentially drift allowing MYI to move into previously FYI covered regions. While this locational exchange is possible, it is a factor that is not accounted for in the present study.

5. Conclusions

The Interactive Multisensor Snow and Ice Mapping System (IMS) was evaluated against several existing sea ice algorithms to determine the feasibility of using IMS for monitoring sea ice phenology. The detection of open water and ice formation, as well as the spatial extent of the sea ice was compared to objectively derived microwave datasets. Additionally, IMS was used to create two new sea ice phenology datasets: melt duration to open water (MD; from melt onset to first open water), and FYI cover duration (ICD; from freeze onset to first open water).

IMS was shown to be advantageous over several automated algorithms available for monitoring sea ice phenology. Using RADARSAT-1 imagery as a visual validation highlighted the strength of IMS to correctly represent the open water in the three selected focus regions, 1) the Amundsen Gulf region (Fig. 2b); 2) the Central Canadian Arctic Archipelago covering the northern route of the Canadian Northwest Passage (Fig. 2c), and 3) the Severnaya Zemlya Archipelago representing one of

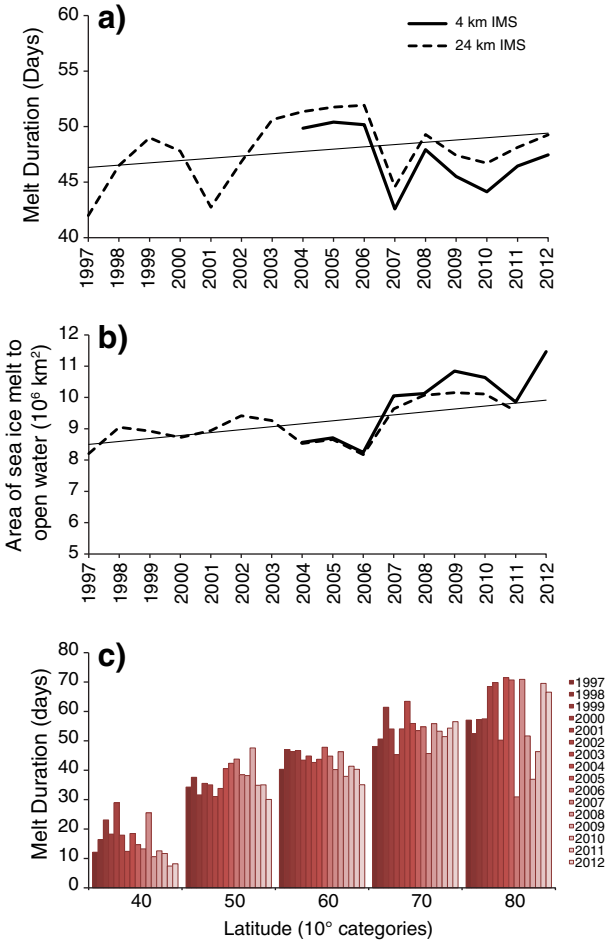

Fig. 14. a) Time series of mean pan-Arctic melt duration to open water and b) time series of total area of sea ice melted to open water and c) mean melt duration (days) by latitude.

the routes of the Northern Sea Route (Fig. 2d). Overall, IMS detects earlier open water and later freeze onset than the automated microwave datasets.

The higher spatial resolution of IMS (4 km) contributes greatly to the improvements over the current passive microwave sea ice estimates by reducing land contamination and allowing the detailed coastal regions to be more accurately represented. Additionally, the detrimental effects of surface winds on the active microwave (i.e. QuikSCAT) retrievals are avoided with IMS. Cloud obstructions and polar darkness can limit the utility of the visible imagery incorporated in IMS, but the inclusion of passive microwave information reduces these issues. Even with the multiple data sources available, problems may still exist in the IMS data, for example August 2012 during the large polar cyclone, IMS appears to overestimate the open water dates compared to the passive microwave estimates during and immediately following the storm. Furthermore, freeze onset is typically more difficult to detect than the transition to open water. Some problems were identified with IMS detecting freeze onset too early for some freshwater lakes in northern Quebec, presumably due to the inclusion of coarse resolution passive microwave during periods of prolonged cloud cover, resulting in unresolved lakes being erroneously identified as snow covered land (Brown & Duguay, 2012). However, the freeze-up of sea ice in the Amundsen Gulf (Fig. 12) shows that IMS data indicate a too late freeze-up (RADARSAT freeze indicated by YD 303, IMS detected freeze on YD306).

IMS can detect the opening and subsequent closing of leads early in the melt season, as well as changes from ice to water later in the season, as multiple transitions from ice to water are possible to identify (while the other datasets using the established algorithms are constituted by only single transitions for melt (or freeze) seasons). The ability to detect leads opening and closing throughout the year provides a useful data source for any studies involving the energy exchange at the ocean–atmosphere interface as the opening of leads could initiate the ice–albedo feedback, progressing melt in that region.

The ability to create melt duration (duration from melt onset to first open water) and FYI cover duration (from freeze onset to first open water) datasets from the daily IMS time series provides new spatial information on sea ice phenology over time. Including the 24 km IMS product to extend the time series from 1997 to 2012 shows a slight increase to the mean FYI MD (2 days decade^{-1}, non-significant), a trend towards longer FYI ICD (5 days decade^{-1}, $p = 0.05$) and an increasing area where sea ice melts to open water (0.1×10^6 km^2 y^{-1}, $\alpha = 0.01$). The trend towards longer ICD in the IMS record can be attributed to the increased area of FYI as more MYI has been replaced with seasonal ice, and experiences shorter open water season at increasingly higher latitudes.

The uses of these new datasets, along with the rest of the phenology datasets from IMS, cross many disciplines, spanning navigation to the validation of model parameters (e.g. melt duration). Forthcoming improvements to the IMS system including the planned inclusion of RADARSAT imagery and the development of a finer resolution IMS product (S. Helfrich, Personal Communication) will serve to further aid the analysts in determining the presence of sea ice throughout the year. While automated, objective microwave algorithms are certainly useful and will continue to be so, the multiple data inputs available to IMS analysts create a very powerful data source for monitoring sea ice variability and change.

Acknowledgments

This research was supported by a NSERC Visiting Fellowship to L. Brown. QuikSCAT SIR and AMSR-E data were obtained from the NASA sponsored Scatterometer Climate Record Pathfinder at Brigham Young University, courtesy of David G. Long. We would like to thank the National Snow and Ice Data Center (NSDIC) for providing the IMS, Sea Ice Index and Concentration data as well as NASA Goddard for the SSM/I data. We would also like to thank the anonymous reviewers who provided useful comments which helped to strengthen the manuscript.

References

Agnew, T., & Howell, S. (2003). The use of operational ice charts for evaluating passive microwave ice concentration data. *Atmosphere-Ocean*, *41*, 317–331, http://dx.doi.org/10.3137/ao.410405.

Barber, D.G., Papakyriakou, T. N., Ledrew, E. F., & Shokr, M. E. (1995). An examination of the relation between the spring period evolution of the scattering coefficient (σ^0) and radiative fluxes over landfast sea-ice. *International Journal of Remote Sensing*, *16*(17), 3343–3363, http://dx.doi.org/10.1080/01431169508954634.

Belchansky, G. I., Douglas, D. C., & Platonov, N. G. (2004). Duration of the Arctic Sea ice melt season: Regional and interannual variability, 1979–2001. *Journal of Climate*, *17*, 67–80.

Brown, L. C., & Duguay, C. R. (2012). Modelling lake ice phenology with an examination of satellite-detected subgrid cell variability. *Advances in Meteorology*, *2012*, 19, http://dx.doi.org/10.1155/2012/529064 (Article ID 529064).

Cavalieri, D. J., Parkinson, C. L., Gloersen, P., Comiso, J. C., & Zwally, H. J. (1999). Deriving long-term time series of sea ice cover from satellite passive-microwave multisensor data sets. *Journal of Geophysical Research*, *104*(C7), 15,803–15,814, http://dx.doi.org/10.1029/1999JC900081.

Cavalieri, D., Parkinson, C., Gloersen, P., & Zwally, H. J. (2008). *Sea ice concentrations from Nimbus-7 SMMR and DMSP SSM/I passive microwave data, 1979–2011*. Boulder, Colorado: National Snow and Ice Data Center (http://nsidc.org/data/nsidc-0051.html).

Chen, C., Lakhankar, T., Romanov, P., Helfrich, S., Powell, A., & Khanbilvardi, R. (2012). Validation of NOAA-Interactive Multisensor Snow and Ice Mapping System (IMS) by comparison with ground-based measurements over continental United States. *Remote Sensing*, *4*, 1134–1145, http://dx.doi.org/10.3390/rs4051134.

Curry, J. A., Schramn, J. L., & Ebert, E. E. (1995). Sea ice–albedo climate feedback mechanism. *Journal of Climate*, *8*, 240–247.

Derksen, C., & Brown, R. (2012). Spring snow cover extent reductions in the 2008–2012 period exceeding climate model projections. *Geophysical Research Letters*, *39*, L19504.

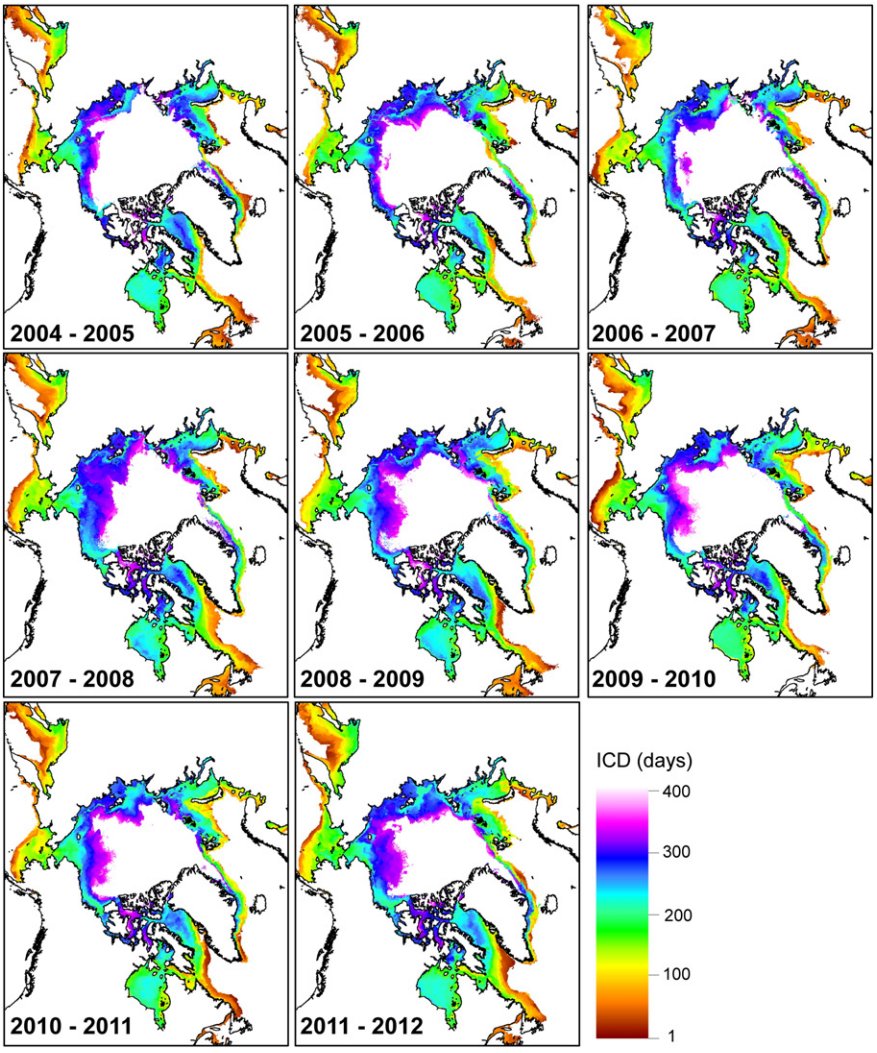

Fig. 15. Ice cover duration (FYI) based on IMS data from freeze onset to the detection of first open water.

Drobot, S. D., & Anderson, M. R. (2001). An improved method for determining snow melt-onset dates over Arctic sea ice using scanning multichannel microwave radiometer and Special Sensor Microwave/Imager data. *Journal of Geophysical Research*, *106*(D20), 24,033–24,049, http://dx.doi.org/10.1029/2000JD000171.

Duguay, C., Brown, L., Kang, K. -K., & Kheyrollah Pour, H. (2011). *Lake ice [in Arctic report card 2011].* (http://www.arctic.noaa.gov/report11/lake_ice.html).

Duguay, C., Brown, L., Kang, K. -K., & Kheyrollah Pour, H. (2012). [The Arctic] lake ice [in "State of the climate in 2011"]. *Bulletin of the American Meteorological Society*, *93*(7), S152–S154.

Duguay, C., Brown, L., Kang, K. -K., & Kheyrollah Pour, H. (2013). [The Arctic] lake ice [In "State of the climate in 2012"]. *Bulletin of the American Meteorological Society*, *94*(8), S124–S126.

Fetterer, F., Knowles, K., Meier, W., & Savoie, M. (2002, updated 2009). *Sea ice index.* Boulder, Colorado USA: National Snow and Ice Data Center. Digital media.

Gogineni, S. P., Moore, R. K., Grenfell, T. C., Barber, D., Digby, S., & Drinkwater, M. (1992). The effects of freeze-up and melt processes on microwave signatures. In F. D. Carsey (Ed.), *Microwave remote sensing of sea ice. Geophys. Monogr. Ser., Vol. 68*. (pp. 329–341). Washington, D. C.: AGU, http://dx.doi.org/10.1029/GM068.

Haarpaintner, J., Tonboe, R., Long, D., & Van Woert, M. (2004). Automatic detection and validity of the sea–ice edge: An application of enhanced-resolution QuikScat/SeaWinds data. *IEEE Transactions on Geoscience and Remote Sensing*, *42*(7), 1433–1443, http://dx.doi.org/10.1109/TGRS.2004.828195.

Helfrich, S. R., McNamara, D., Ramsay, B. H., Baldwin, T., & Kasheta, T. (2007). Enhancements to, and forthcoming developments in the Interactive Multisensor Snow and Ice Mapping System (IMS). *Hydrological Processes*, *21*, 1576–1586.

Howell, S. E. L., Brown, L. C., Kang, K. K., & Duguay, C. R. (2009). Variability in Ice Phenology on Great Bear Lake and Great Slave Lake, NWT, from SeaWind/QuikSCAT: 2000–2006. *Remote Sensing of the Environment*, *113*, 816–834.

Howell, S. E. L., Derksen, C., & Tivy, A. (2010). Development of a water clear of sea ice detection algorithm from enhanced SeaWinds/QuikSCAT and AMSR-E measurements. *Remote Sensing of Environment*, *114*, 2594–2609.

Howell, S. E. L., Tivy, A., Yackel, J. J., Else, B. G. T., & Duguay, C. R. (2008). Changing sea ice melt parameters in the Canadian Arctic Archipelago: Implications for the future presence of multiyear ice. *Journal of Geophysical Research*, *113*, C09030, http://dx.doi.org/10.1029/2008JC004730.

Hudson, S. R., Granskog, M.A., Sundfjord, A., Randelhoff, A., Renner, A. H. H., & Divine, D.V. (2013). Energy budget of first-year Arctic sea ice in advanced stages of melt. *Geophysical Research Letters*, *40*, 2679–2683, http://dx.doi.org/10.1002/grl.50517.

Kang, K. -K., Duguay, C. R., & Howell, S. E. L. (2012). Estimating ice phenology on large northern lakes from AMSR-E: Algorithm development and application to Great Bear Lake and Great Slave Lake, Canada. *The Cryosphere*, *6*(2), 235–254.

Kwok, R., Cunningham, G. F., & Nghiem, S. V. (2003). A study of melt onset in RADARSAT SAR imagery. *Journal of Geophysical Research*, *108*(C11), 3363, http://dx.doi.org/10.1029/2002JC001363.

Long, D.G., Hardin, P. J., & Whitling, P. T. (1993). Resolution enhancement of spaceborne scatterometer data. *IEEE Transactions in Geoscience and Remote Sensing*, *31*(3), 700–715.

Long, D.G., & Hicks, B. R. (2005). *Standard BYU QuikSCAT/SeaWinds land/ice image products, report.* Provo, Utah: Brigham Young University (30 pp.).

Markus, T., Stroeve, J. C., & Miller, J. (2009). Recent changes in Arctic sea ice melt onset, freeze up, and melt season length. *Journal of Geophysical Research*, *114*, C12024, http://dx.doi.org/10.1029/2009JC005436.

Maslanik, J., Stroeve, J., Fowler, C., & Emery, W. (2011). Distribution and trends in Arctic sea ice age through spring 2011. *Geophysical Research Letters*, *38*, L13502, http://dx.doi.org/10.1029/2011GL047735.

Mortin, J., Howell, S. E. L., Wang, L., Derksen, C., Svensson, G., Graversen, R. G., et al. (2014). Extending the QuikSCAT record of seasonal melt–freeze transitions over Arctic sea ice using ASCAT. *Remote Sensing of Environment*, *141*, 214–230, http://dx.doi.org/10.1016/j.rse.2013.11.004.

Mortin, J., Schrøder, T. M., Walløe Hansen, A., Holt, B., & McDonald, K. C. (2012). Mapping of seasonal freeze–thaw transitions across the pan-Arctic land and sea ice domains with satellite radar. *Journal of Geophysical Research*, *117*, C08004, http://dx.doi.org/10.1029/2012JC008001.

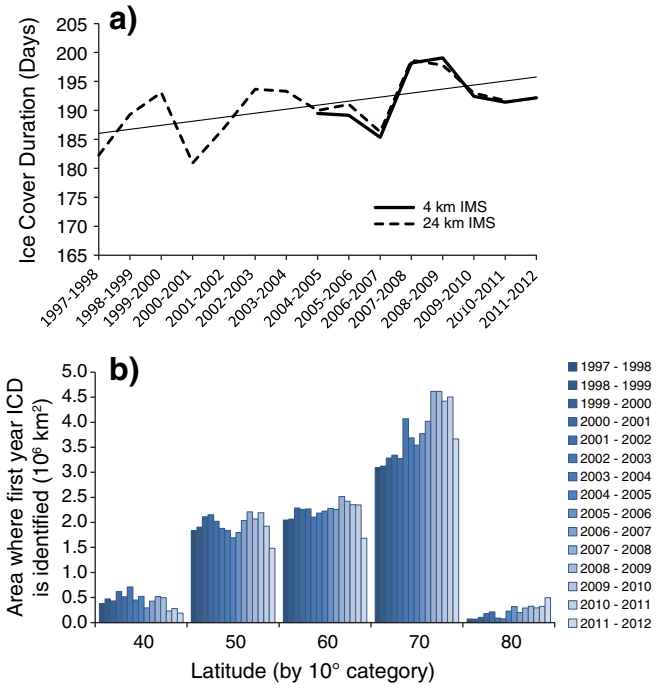

Fig. 16. a) Time series of mean pan-Arctic FYI cover duration and b) the total area, by latitude, where ICD was identified (areas which experienced both freeze and melt each year).

National Ice Center (2008, updated daily). *IMS daily Northern Hemisphere snow and ice analysis at 4 km and 24 km resolution.* Boulder, CO: National Snow and Ice Data Center. Digital media.

NSDIC (2006, updated 2011). Sea ice concentration documentation. available online: http://nsidc.org/data/docs/daac/nsidc0051_gsfc_seaice.gd.html

NSIDC (2008, updated 2013). Sea ice index documentation. available online: http://nsidc.org/data/docs/noaa/g02135_seaice_index/index.html

NSIDC (2011). IMS data description. available online: http://nsidc.org/data/docs/noaa/g02156_ims_snow_ice_analysis/index.html

Parkinson, C. L., & Comiso, J. C. (2013). On the 2012 record low Arctic sea ice cover: Combined impact of preconditioning and an August storm. *Geophysical Research Letters*, *40*, 1356–1361, http://dx.doi.org/10.1002/grl.50349.

Perovich, D. K., Light, B., Eicken, H., Jones, K. F., Runciman, K., & Nghiem, S. V. (2007). Increasing solar heating of the Arctic Ocean and adjacent seas, 1979–2005: Attribution and role in the ice–albedo feedback. *Geophysical Research Letters*, *34*, L19505, http://dx.doi.org/10.1029/2007GL031480.

Perovich, D. K., Nghiem, S. V., Markus, T., & Schweiger, A. (2007). Seasonal evolution and interannual variability of the local solar energy absorbed by the Arctic sea ice–ocean system. *Journal of Geophysical Research*, *112*, C03005, http://dx.doi.org/10.1029/2006JC003558.

Ramsay, B. H. (1998). The interactive multisensor snow and ice mapping system. *Hydrological Processes*, *12*, 1537–1546.

Scott, K. A., Buehner, M., Caya, A., & Carrieres, T. (2013). A preliminary evaluation of the impact of assimilating AVHRR data on sea ice concentration analyses. *Remote Sensing of Environment*, *128*, 212–223.

Simmonds, I., & Rudeva, I. (2012). The great Arctic cyclone of August 2012. *Geophysical Research Letters*, *39*, L23709, http://dx.doi.org/10.1029/2012GL054259.

Smith, D.M. (1998). Observation of perennial Arctic sea ice melt and freeze-up using passive microwave data. *Journal of Geophysical Research*, *103*, 27,753–27,769, http://dx.doi.org/10.1029/98JC02416.

Stiles, W. H., & Ulaby, F. T. (1980). The active and passive microwave response to snow parameters: 1. Wetness. *Journal of Geophysical Research*, *85*(C2), 1037–1044, http://dx.doi.org/10.1029/JC085iC02p01037.

Wang, L., Wolken, G., Sharp, M., Howell, S., Derksen, C., Brown, R., et al. (2011). Integrated pan-Arctic melt onset detection from satellite active/passive microwave measurements, 2000–2009. *Journal of Geophysical Research*, *116*, D22103, http://dx.doi.org/10.1029/2011JD016256.

Winebrenner, D. P., Holt, B., & Nelson, E. D. (1996). Observation of autumn freeze-up in the Beaufort and Chukchi seas using the ERS 1 synthetic aperture radar. *Journal of Geophysical Research*, *101*(C7), 16,401–16,419.

Winebrenner, D. P., Nelson, E. D., Colony, R., & West, R. D. (1994). Observation of melt onset on multiyear Arctic sea ice using ERS 1 synthetic aperture radar. *Journal of Geophysical Research*, *99*(C11), 22425–22441 (http://onlinelibrary.wiley.com/doi/10.1029/94JC01268/abstract).

Yackel, J. J., Barber, D.G., & Papakyriakou, T. N. (2001). On the estimation of spring melt in the North Water Polynya using RADARSAT-1. *Atmosphere-Ocean*, *39*, 195–208.

Yu, P., Clausi, D. A., & Howell, S. E. L. (2009). Fusing AMSR-E and QuikSCAT imagery for improved sea ice recognition. *IEEE Transactions on Geoscience and Remote Sensing*, *47*(7), 1980–1990, http://dx.doi.org/10.1109/TGRS.2009.2013632.